BIOCHEMISTRY
including biophysical chemistry & molecular biology
Article

Biochemistry **2010,** *49,* 2297–2304 2297
DOI: 10.1021/bi902157b

Temperature and pH Dependence of Enzyme-Catalyzed Hydrolysis of *trans*-Methylstyrene Oxide. A Unifying Kinetic Model for Observed Hysteresis, Cooperativity, and Regioselectivity[†]

Diana Lindberg, Mario de la Fuente Revenga,[‡] and Mikael Widersten*

Department of Biochemistry and Organic Chemistry, Uppsala University, BMC, Box 576, SE-751 23 Uppsala, Sweden.
[‡]Current affiliation: Instituto de Quimica Medica-CSIC, Juan de la Cierva 3, E-28006 Madrid, Spain.

Received December 16, 2009; Revised Manuscript Received February 9, 2010

ABSTRACT: The underlying enzyme kinetics behind the regioselective promiscuity shown by epoxide hydrolases toward certain epoxides has been studied. The effects of temperature and pH on regioselectivity were investigated by analyzing the stereochemistry of hydrolysis products of (1*R*,2*R*)-*trans*-2-methylstyrene oxide between 14−46 °C and pH 6.0−9.0, either catalyzed by the potato epoxide hydrolase StEH1 or in the absence of enzyme. In the enzyme-catalyzed reaction, a switch of preferred epoxide carbon that is subjected to nucleophilic attack is observed at pH values above 8. The enzyme also displays cooperativity in substrate saturation plots when assayed at temperatures ≤30 °C and at intermediate pH. The cooperativity is lost at higher assay temperatures. Cooperativity can originate from a kinetic mechanism involving hysteresis and will be dependent on the relationship between k_{cat} and the rate of interconversion between two different Michaelis complexes. In the case of the studied reactions, the proposed different Michaelis complexes are enzyme−substrate complexes in which the epoxide substrate is bound in different binding modes, allowing for separate pathways toward product formation. The assumption of separated, but interacting, reaction pathways is supported by that formation of the two product enantiomers also displays distinct pH dependencies of k_{cat}/K_M. The thermodynamic parameters describing the differences in activation enthalpy and entropy suggest that (1) regioselectivity is primarily dictated by differences in activation entropy with positive values of both $\Delta\Delta H^{\ddagger}$ and $\Delta\Delta S^{\ddagger}$ and (2) the hysteretic behavior is linked to an interconversion between Michaelis complexes with rates increasing with temperature. From the collected data, we propose that hysteresis, regioselectivity, and, when applicable, hysteretic cooperativity are closely linked properties, explained by the kinetic mechanism earlier introduced by our group.

Epoxides are important compounds in the synthesis of fine chemicals and pharmaceutical intermediates (*1*). Epoxide hydrolases facilitate ring-opening reactions of the epoxide ring structure, incorporating a water to yield a vicinal diol. The soluble epoxide hydrolase (EC 3.3.2.10) from *Solanum tuberosum*, StEH1, belongs to the structural family of α/*β*-hydrolase fold enzymes (*2*). The chemical mechanism of α/*β*-hydrolase fold epoxide hydrolases involves the formation of a covalent alkyl enzyme intermediate resulting from a nucleophilic attack by an Asp carboxylate on one of the oxirane carbons, facilitated by tyrosine phenols hydrogen-bonded to the epoxide oxygen. The reaction is concluded by a base-catalyzed hydrolysis of the alkyl enzyme intermediate into the vicinal diol product (*3*−*6*). The extent of selectivity shown by epoxide hydrolases for different epoxide substrate stereoisomers is dependent on (1) the enantioselectivity and (2) the regioselectivity shown in the initial nucleophilic attack on the oxirane ring (Figure 1).

The regioselectivity toward a specific epoxide is influenced by the epoxide hydrolase catalyst and by intrinsic properties of the substrates (*7*−*29*). 1,1-Disubstituted aliphatic epoxides are primarily attacked at the least hindered carbon while the regioselectivity for mono- or 1,2-disubstituted aliphatic substrates may differ between substrate enantiomers (*29*). The selectivity of the reactions with phenyl-substituted epoxides are more complicated to predict due to the ability of the phenyl ring to stabilize a carbocation-like reaction intermediate (*15*, *30*, *31*). StEH1 displays a relatively broad substrate specificity range but with a preference for aliphatic and aromatic *trans*-substituted epoxides (*3*, *12*, *32*−*37*). While the enzyme shows a high degree of regioselectivity with most compounds, it displays promiscuous behavior in the hydrolysis of certain aryl epoxides. In the present context, *promiscuity* implies that the enzyme may catalyze attack at either electrophilic carbon of the epoxide ring. A clear-cut example is the transformation of styrene oxide, where the (*S*)-enantiomer is attacked at the more stabilized benzylic carbon whereas the (*R*)-isomer is almost exclusively reacting at the sterically least hindered aliphatic carbon (*37*). With *trans*-2-methylstyrene oxide (2-MeSO), the (1*S*,2*S*)-enantiomer (**1**) is exclusively attacked at the benzylic carbon while the (1*R*,2*R*)-enantiomer (**2**) is opened at either carbon (Figure 1) (*12*). A similar promiscuity with the 2-MeSO epoxide is also observed in reactions catalyzed by a cress epoxide hydrolase (AtEH) and by other isoenzymes (*7*, *11*, *13*, *38*, *39*). Notably, in the AtEH-catalyzed reaction the enantiospecificity is reversed as compared to the StEH1 reaction; **2** is exclusively reacting at the benzylic

[†]This work was supported by The Swedish Research Council, The Carl Trygger Foundation, and The O. E. and Edla Johansson Foundation.

*Corresponding author. E-mail: mikael.widersten@biorg.uu.se. Phone: +46 (0)18 471 4992. Fax: +46 (0)18 55 8431.

Published on Web 02/10/2010

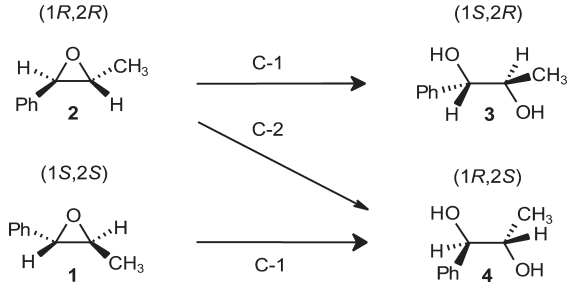

FIGURE 1: Stereoselective outcome of StEH1-catalyzed reaction of the two enantiomers of *trans*-2-MeSO. The StEH1 regioselectivity toward **1** is >98% in preference of C-1, while for enantiomer **2** the enzyme shows regioselective promiscuity and prefers C-1 to C-2 with a factor of 2:1 at pH 7.5, 30 °C.

Scheme 1

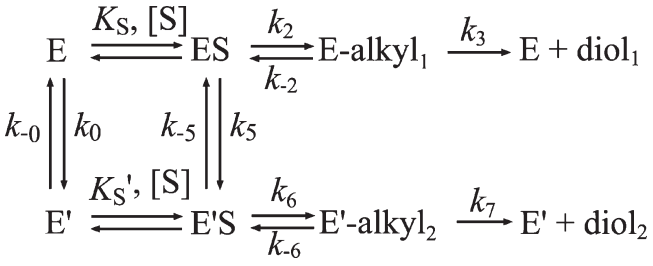

epoxide carbon whereas **1** is attacked at either carbon with low preference (*13*, *38*). Theoretical investigations on the reaction with 2-MeSO catalyzed by the murine soluble epoxide hydrolase suggest that regioselectivity is dependent on a hydrogen bond between one of the active site tyrosines with the substrate epoxide oxygen (*13*, *40*). The results from the molecular dynamics simulations by Schøitt and Bruice proposed that the rigidness of the active site is important in determining the degree of regioselectivity, with a tight active site conformation favoring a higher degree of regioselectivity (*40*).

A kinetic mechanism explaining the formation of both the (1*S*,2*R*), **3**, and (1*R*,2*S*), **4**, diols produced in StEH1-catalyzed transformation of **2** is shown in Scheme 1. The model includes different interconverting forms of the substrate-free enzyme as well as the Michaelis complexes. The distinct alkyl enzyme intermediates, resulting from attack at either C-1 or C-2, are subsequently hydrolyzed into the different diol products.

The enzyme displays a hysteretic behavior with both enantiomers of 2-MeSO, as seen in the pre-steady-state measurements, which indicates the existence of different enzyme forms (*12*). The conformational changes coupled to the hysteretic behavior are supported by theoretical studies on the murine EH; MD simulations of a 4 ns time span following formation of the Michaelis complex show anticorrelated motion of the lid and core domains across the active site during catalysis (*41*).

Regio- and enantioselectivity are closely linked components of epoxide hydrolase catalysis, both influencing the stereochemical purity of the product. Substrate selectivity in enzyme catalysis, be it structural or enantio- or regioselectivity, is determined by interplaying factors intrinsic to the reacting system. The enantioselectivity is also affected by external conditions such as temperature, pH, pressure, and composition of the reaction medium (*42*, *43*). In this work, we have studied the regioselectivity of StEH1 in greater detail by examining how regioselectivity is affected by changes in temperature and pH. Kinetic studies in the steady-state and the pre-steady-state phases, in combination with quantitative measurements of product diol ratios, have allowed us to extract kinetic parameters for formation of the individual product enantiomers starting from the same substrate enantiomer. The study also aimed at investigating possible linkages between conformational changes in the enzyme, hysteresis, and degree of regioselectivity.

EXPERIMENTAL PROCEDURES

Chemicals, Reagents, and General Procedures. 2-MeSO and other chemicals were purchased from Aldrich at the highest available purity. The StEH1 enzyme was overexpressed in *Escherichia coli* XL1 Blue cells (Stratagene) and purified according to a previously described protocol (*3*). Once purified, the proteins retained full activity upon storage at 4 °C over the time period of analysis. In the HPLC measurements, separation of analytes was performed over a Daicel Chiralpak AD-H (250 × 4.6 mm i.d.) using a Shimadzu LC10 pump. Substrates were injected with a Shimadzu SIL-10AF autosampler, and peaks were detected at 220 nm using a Shimadzu SPDM20A diode array detector.

The change in the molar absorbance resulting from hydrolysis of 2-MeSO to diols was determined by subtracting the UV spectrum of the formed diol, at equilibrium, from that of the epoxide, obtaining a molar extinction coefficient of $\Delta\varepsilon = -4.3\ \mathrm{mM^{-1}\,cm^{-1}}$. The equilibrium absorbance of the diol was achieved by hydrolyzing 0.2 mM **1** to completion in the presence of 0.4 μM StEH1 in 0.1 M sodium phosphate, pH 7.5. Buffer pH was adjusted by adding either NaOH or H_3PO_4 to the sodium phosphate solution. All curve fitting and data statistic analyses were performed with programs MMFIT, INRATE, RFFIT, LINFIT, or QNFIT in the SIMFIT package (http://www.simfit.man.ac.uk).

Steady-State Kinetics. The activity during the steady state was measured spectrophotometrically in 0.1 M sodium phosphate buffer, pH 7.5, at substrate concentrations ranging from 20 to 250 μM at 22, 30, 38, and 46 °C. A decrease in activity at high temperatures is expected to be linked to kinetics only, and not to stability issues, as the $t_{1/2}$ at 45 °C is >500 min. The substrate was dissolved in acetonitrile and added to the buffer at a final concentration of 1% (v/v) acetonitrile. Enzyme was diluted in 0.1 M sodium phosphate, pH 7.5, and was added to the reaction mixture at a final concentration of 400 nM. The rate of uncatalyzed epoxide hydrolysis was below the detection limit during the assays.

Kinetic parameters k_{cat} and K_M were extracted after fitting the Michaelis−Menten equation by nonlinear regression (MMFIT) to the experimental data. For the parameters k_{cat}, $K_{0.5}$, and n_H (the Hill coefficient) a rational function with a floating exponent was fitted to the initial rate data determined at 22 and 30 °C for **2** using INRATE.

The derived steady-state rate law for formation of the sum of diol products, following the mechanism in Scheme 1, is described by a second-order expression in the form of eq 1 (*44*).

$$v_0 = \frac{i[\mathrm{S}]^2 + j[\mathrm{S}]}{k + l[\mathrm{S}]^2 + m[\mathrm{S}]} \quad (1)$$

An evaluation of the individual parameters of eq 1 is presented in the Supporting Information.

Steady-State Parameters for Formation of Individual Diols. The steady-state kinetics of StEH1-catalyzed hydrolysis of **2** was followed at 22 and 38 °C, pH of 7.5, in the presence of 135−760 μM epoxide. The concentration for the sum of diols formed was first determined spectrophotometrically, in triplicate. Reactions were terminated with the addition of methanol to a

Table 1: Steady-State and Pre-Steady-State Parameters for StEH1-Catalyzed Hydrolysis of **2** at pH 7.5

	MM equation			Hill equation				pre steady state
T (°C)	k_{cat} (s^{-1})	K_M (mM)	k_{cat}/K_M (s^{-1} mM^{-1})	k_{cat} (s^{-1})	$K_{0.5}$ (mM)[a]	$k_{cat}/K_{0.5}$ (s^{-1} mM^{-1})	n_H[b]	$k_5 + k_{-5}$ (s^{-1})
22	6.9 ± 3	1.6 ± 0.8	4.3 ± 3	1.4 ± 0.2	0.17 ± 0.03	8.2 ± 2	1.7 ± 0.2	6.7 ± 0.8
30	4.7 ± 0.7	0.49 ± 0.1	9.7 ± 2	3.0 ± 0.6	0.22 ± 0.08	14 ± 6	1.2 ± 0.2	12 ± 2
38	4.8 ± 1	0.61 ± 0.2	7.9 ± 3				(1)	51 ± 3
46	10 ± 5	1.2 ± 0.6	8.3 ± 6				(1)	66 ± 5

[a]The substrate concentration resulting in $v_0 = V_{max}/2$. $K_{0.5} = K_M$ if $n = 1$. [b]Hill coefficient.

final concentration of 50%, whereafter solvent was evaporated. After resolvation of the residue in a 80/20 hexane/2-propanol mixture, the ratio of each diol was obtained by chiral HPLC, in duplicate measurements. The total concentration of diols together with the molar ratios allowed for calculations of the absolute concentrations of the individual diols at each time point. Steady-state kinetic parameters were determined by fitting the Michaelis−Menten equation to the data.

Pre-Steady-State Kinetics. Data were collected with an Applied Photophysics SX.20MV sequential stopped-flow spectrophotometer at different temperatures (22, 30, 38, or 46 °C) in a 0.1 M sodium phosphate solution at pH 7.5. The concentration of **2** was varied between 85 and 750 μM, with an StEH1 concentration of 10 μM. The substrate was dissolved in acetonitrile before being added to the reaction mixture, resulting in a final acetonitrile concentration of 1% (v/v). The catalyzed reaction was followed as a decay in the intrinsic tryptophan fluorescence, excitation λ 290 nm, collecting the emitted light after passage through a 320 nm cutoff filter. Pre-steady-state kinetic parameters were determined from multiple-turnover experiments under pseudo-first-order conditions, with a minimum of two repetitions of eight fluorescence traces being collected, all of which were averaged for the different substrate concentrations. The apparent rates, k_{obs}, were determined by fitting a single exponential function with a floating end point, $f = A \exp(-k_{obs}t) + C$, where f is the averaged fluorescent trace, A the amplitude, t the time, and C the floating end point. Values of the rate sum ($k_5 + k_{-5}$) (Scheme 1) were obtained after fitting experimental values to eq SI-1 (see Supporting Information) (*12*, *45*, *46*).

Regioselectivity. The distribution of diol products was analyzed by chiral HPLC. Hydrolysis of **2** was conducted at different temperatures (14, 22, 30, 38, or 46 °C) in 50 mM sodium phosphate buffer adjusted to pH values ranging from pH 6.0 to pH 9.0. The reaction mixtures contained a final concentration of 1% (v/v) acetonitrile in a total volume of 1 mL. In the enzyme-catalyzed reactions a concentration of 0.1 μM StEH1 was used, with a concentration of **2** of 0.185 mM. Reactions were terminated by adding methanol to a final concentration of 50% (v/v). In all enzymatic reactions, at all temperatures and pH values, the products from the nonenzymatic reactions constituted less than 1% of the total product yield. The nonenzymatic reactions were conducted with 14.5 mM **2** in a 50 mM sodium phosphate buffer and 3% (v/v) acetonitrile. The reactions were terminated at a time period suitable for determination of the quantitative relationship of both diols (24−48 h). Following hydrolysis, water was evaporated from the reaction mixture. The residue was dissolved in 200 μL of hexane/2-propanol (85/15). The diols, dissolved in organic solvent, were separated by chiral HPLC. The enzymatic reactions were performed in duplicate while the nonenzymatic reactions were performed once. The HPLC analyses were repeated twice for all reactions.

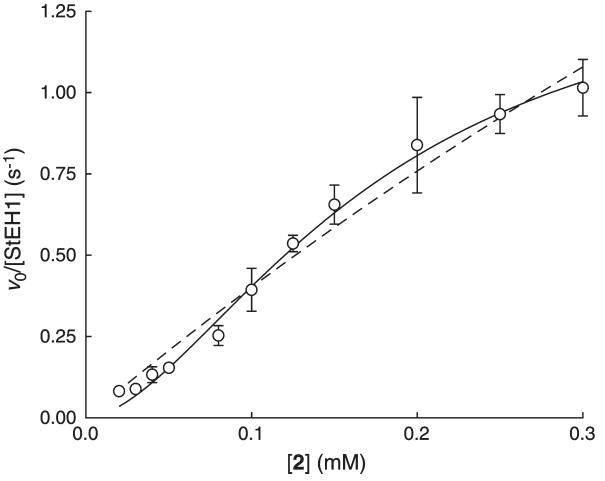

FIGURE 2: Initial steady-state velocities as a function of varying concentrations of epoxide **2** in StEH1-catalyzed hydrolysis at 22 °C, pH 7.5. The Michaelis−Menten equation (dashed line) and a Hill equation (solid line), with a Hill coefficient of 1.7, were fitted to the data. Error bars represent standard deviations, $n \geq 3$.

Difference in Enthalpic and Entropic Contributions to the Activation Energy. The difference in activation enthalpy and entropy of the different transition states of the two pathways leading to the formation of the two product enantiomers was calculated from

$$\Delta\Delta G^{\ddagger} = \Delta G^{\ddagger}_{\mathbf{3}} - \Delta G^{\ddagger}_{\mathbf{4}} = -RT \ln E \quad (2)$$

where $\Delta\Delta G^{\ddagger}$ is the free energy of activation, R the universal gas constant, T the absolute temperature, and

$$\Delta\Delta G^{\ddagger} = \Delta\Delta H^{\ddagger} - T\Delta\Delta S^{\ddagger} \quad (3)$$

Combining (2) and (3) allows for extraction of the equation

$$\ln((k_{cat}/K_M)^{\mathbf{3}}/(k_{cat}/K_M)^{\mathbf{4}}) = -(\Delta_{\mathbf{3-4}}\Delta H^{\ddagger})/(RT) + \Delta_{\mathbf{3-4}}\Delta S^{\ddagger}/R \quad (4)$$

where $\Delta_{\mathbf{3-4}}\Delta H$ is defined as the difference in activation enthalpy and $\Delta_{\mathbf{3-4}}\Delta S$ the difference in activation entropy for the product enantiomers.

RESULTS AND DISCUSSION

Hysteretic Cooperativity. Steady-state kinetics of the catalyzed hydrolysis of **2** (Figure 1) was analyzed at temperatures ranging from 22 to 46 °C, at pH 7.5. The reaction product is the sum of diols formed following attack at either of the epoxide carbons and, thus, does not resolve the individual rates of formation of the different enantiomers. At 22 and 30 °C the substrate dependence of the initial velocities showed poor fits to the Michaelis−Menten model, instead displaying a cooperative

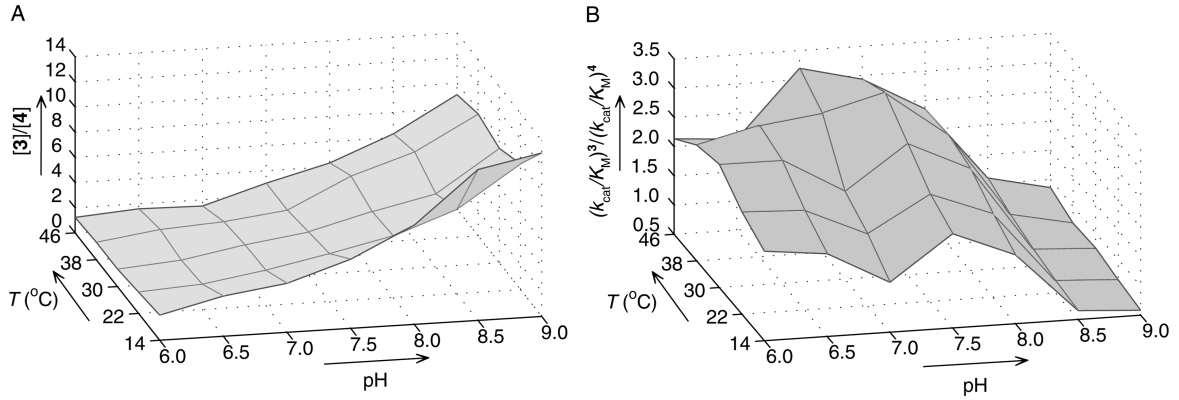

FIGURE 3: Ratio of the phenylpropyl-1,2-diols **3** and **4** as a function of temperature and pH, expressed in (A) [**3**]/[**4**] after the noncatalyzed reactions and (B) the ratio of the specificity constants, $(k_{cat}/K_M)^3/(k_{cat}/K_M)^4$, of StEH1-catalyzed hydrolysis of **2**.

behavior (Figure 2, Table 1). As a result, the Michaelis constants could not be determined accurately and were replaced by an arbitrary constant, $K_{0.5}$, defined as the substrate concentration at $V_{max}/2$. At 30 °C, cooperativity was less pronounced. At the higher temperatures, cooperativity was completely absent, and the reactions were well modeled by the Michaelis−Menten equation, with $K_{0.5} \equiv K_M$. The values of the individual kinetic parameters k_{cat} and $K_{0.5}$ increased in a compensatory manner with increasing temperature, resulting in essentially unaltered catalytic efficiencies (Table 1).

Cooperativity is linked to changes in enzyme structure and is common in allosterically regulated enzymes. There has been no earlier report on observed cooperative behavior among epoxide hydrolases, however, although authors have reported on deviations from Michaelis−Menten kinetics in steady-state measurements (*25*). Cooperativity in monomeric enzymes may arise from the presence of slow reaction steps on the reaction pathway. In this context "slow" means "on the same time scale as k_{cat}". On the basis of results from pre-steady-state kinetic analysis of catalyzed hydrolysis of the two enantiomers of *trans*-2-MeSO we previously proposed that StEH1 undergoes slow conformational changes induced by the substrate (Scheme 1). The link between cooperativity in monomeric enzymes and the concept of hysteretic enzymes with slow conformational changes has been established. The term hysteretic cooperativity has been coined to distinguish this from cooperativity resulting from changes in the quaternary structure of multimeric allosteric enzymes. Requiring the presence of the two states of free enzyme or enzyme−ligand complexes, as depicted in Scheme 1, cooperativity arises as a result of a shift of the dominant pathway with increasing substrate concentrations. The presence of both hysteretic and cooperative behavior is not necessarily linked and depends on the actual values of the rate constants (*47*, *48*).

From the derived rate law for Scheme 1 (eq 1), it can be deduced that if the value of k_{-5} increases to a large value, the steady-state rate equation is simplified to become

$$v_0 = \frac{i[S]^2}{l[S]^2 + m[S]} \quad (5)$$

i.e.

$$v_0 = \frac{i[S]}{l[S] + m} \quad (6)$$

Dividing numerator and denominator by l results in the Michaelis−Menten equation with k_{cat} defined by i/l and K_M by m/l. The dependence, in terms of the individual microscopic rate constants in Scheme 1, of each parameter in eqs 5 and 6 is provided in the Supporting Information.

This behavior is in correspondence to our experimental results. One of the prerequisites for hysteretic cooperativity, as defined by Neet and Ainslie, is that the slow transition must be of a rate lower or as low as the maximum velocity of the system (*47*). As the Hill coefficient decreases from a maximum value of 1.7 at 22 °C (pH 7.5) to no observable cooperativity at 38 °C, the sum of rate constants for interconversion between the ES and E′S complexes ($k_5 + k_{-5}$) seen from the pre-steady-state measurements increases with increasing temperature (Table 1). We propose that this gradually lesser contribution of the rates between the Michaelis complexes ES and E′S ($k_5 + k_{-5}$) to k_{cat} with increasing temperatures is the reason why hysteretic cooperativity is lost with increasing temperatures. At lower temperatures, the value of $k_5 + k_{-5}$ is comparable to the value of k_{cat}; i.e., at this temperature either k_5 or k_{-5} can potentially constitute a rate-limiting step for one pathway leading to a specific product diol. As the sum of $k_5 + k_{-5}$ increases with temperature, these rates would become less influential on the resulting k_{cat}.

Catalytic Efficiency and Regioselectivity. The initial rates of formation of the individual product diols from hydrolysis of **2** were determined. Measurements were performed in the presence or absence of StEH1 (Supporting Information Tables SI-1 and SI-2) in a pH range of 6.0−9.0, within a temperature interval of 14−46 °C.

In the nonenzymatic hydrolysis the ratios of diols were compared over the pH and temperature interval (Figure 3A). If assuming an inversion of configuration takes place as a consequence of an S_N2-type reaction, the general trend is an increased preference for ring opening at the aliphatic carbon (*30*, *49*). At a low pH and higher temperature this results in an essentially racemic mixture of products. Higher pH values and lower temperatures direct ring opening toward the benzylic carbon; at pH 9.0 and 14 °C the enantiomeric excess of **3** is 86%, corresponding to a molar ratio of 13:1. This is in accordance with results from other groups, at intermediate temperatures (28 and 30 °C), both in a buffered solution and in water (*23*, *37*).

For the enzymatic reactions the dependence on pH and temperature is considerably different. The ratios of the specificity constants for each diol, $(k_{cat}/K_M)^3/(k_{cat}/K_M)^4$, under these conditions are shown in Figure 3B. In general, the overall sensitivity to changes in pH and temperature is less pronounced as compared to the nonenzymatic reaction. Neutral pH conditions and higher temperatures favor ring opening at the benzylic C-1, whereas at a pH ≥8.5 C-2 is preferentially attacked.

To further resolve the individual contributions of the pathways leading to each of the diol products, the kinetics of formation of the individual diol enantiomers were followed for a chosen set of temperatures at pH 7.5. A comparison of the k_{cat} values for formation of each individual diol product (Table 2) with those determined for the combined formation of both diols (Table 1) reveals that, at this pH, the factors contributing to increased selectivity for C-1, to produce diol **3**, result in a lowered K_M value at the higher assay temperatures. This results in an overall higher value of k_{cat}/K_M for formation of that diol (Table 2).

pH Dependence in Regioselectivity. Plots of the extracted k_{cat}/K_M values against pH (Figure 4) show that the enzyme-facilitated ring opening at C-1 is dependent on titration of both a base and an acid, with apparent pK_a values of approximately 6.7 for the conjugate acid of the catalytic base, and 8.2, respectively, at all temperatures (Table 3). The ring opening at C-2, on the other hand, is solely dependent on the titration of a catalytic base to reach maximum activity, with an apparent pK_a value of approximately 6.5 of its conjugate acid. The presence of an acid titrating with a pK_a > 10 would escape detection in this study and cannot be excluded at this point. The absence of an acid titration can also be an effect of that the acid-dependent reaction step in the pathway leading to diol **3** is not rate limiting for k_{cat}/K_m in the reaction leading to diol **4**.

We propose that in the two pathways leading to the formation of diols **3** and **4**, the substrate is positioned in two different binding modes. Theoretical calculations support the supposedly different binding modes on the related human soluble epoxide hydrolase (HssEH). The largest structural differences found between the potato and human enzymes are located in the lid domains. The two active sites differ somewhat in size and shape of the cavities in the vicinity of the respective Asp nucleophiles, but the differences are mainly found at the outer margins of these cavities (*50*). When Hopmann and Himo positioned the 2-MeSO substrate in the active site of HssEH, aiming to create a local energy minimum to facilitate nucleophilic attack at C-2 in the initial alkyl enzyme forming step, this required a rearrangement of the substrate pose in the active site cavity as compared to a reaction involving attack at C-1. Furthermore, a 180° repositioning of the substrate phenyl group to facilitate attack at either carbon was almost identical in energy as compared to the original binding model (*51*). The same possibility to bind in two opposite angles in the active site cavity was also observed using the same substrate in theoretical studies with the murine epoxide hydrolase (*49*).

The possibility of perturbed pK_a values of catalytic acids has been addressed in theoretical studies on HssEH and StEH1. The results proposed that the acid titrated in the basic limb of the pH profile is the imidazolium form of His300 (StEH1 numbering), which also serves as the general base of the catalytic triad in its deprotonated form (*51*, *52*). These investigations give at hand that the dissociation of the tetrahedral intermediate formed during hydrolysis of the alkyl enzyme is dependent on a concerted protonation of the leaving group oxyanion by His300 in its imidazolium state. Furthermore, based on the kinetic behavior of an active site mutant enzyme and computer simulations, Thomaeus et al. suggest that these perturbations in pK_a of His300 result from electrostatic changes in the active site microenvironment over the catalytic cycle (*52*). Assuming that epoxide **2** can be positioned in two different positions within the active site, this can be expected to influence the electrostatics in a analogous way as a consequence to differences in interaction patterns within the active site in the different pathways leading to the two product

Table 2: Steady-State Kinetic Parameters for StEH1-Catalyzed Formation of **3** and **4** at pH 7.5

	k_{cat} (s^{-1})		K_M (mM)		k_{cat}/K_M (s^{-1} mM^{-1})	
T (°C)	diol **3**	diol **4**	diol **3**	diol **4**	diol **3**	diol **4**
22	3.2 ± 0.4	> 0.7[a]	1.5 ± 0.2	> 0.5[a]	2.1 ± 0.1	0.89 ± 0.04
38	2.8 ± 0.3	> 0.8[a]	0.52 ± 0.1	> 0.5[a]	5.5 ± 1	1.1 ± 0.6

[a]No substrate saturation kinetics within the concentration range used.

Table 3: Apparent pK_a Values of k_{cat}/K_M for Formation of Diols **3** and **4** in StEH1-Catalyzed Hydrolysis of **2** at Different Temperatures

	3		**4**
T (°C)	pK_{a1}	pK_{a2}	pK_a
14	7.0 ± 0.3	8.1 ± 0.3	6.4 ± 0.2
22	6.8 ± 0.04	8.2 ± 0.2	6.6 ± 0.1
30	6.7 ± 0.3	8.1 ± 0.4	6.5 ± 0.2
38	6.4 ± 0.2	8.6 ± 0.2	6.6 ± 0.2
46	6.5 ± 0.3	8.2 ± 0.4	6.0 ± 0.2

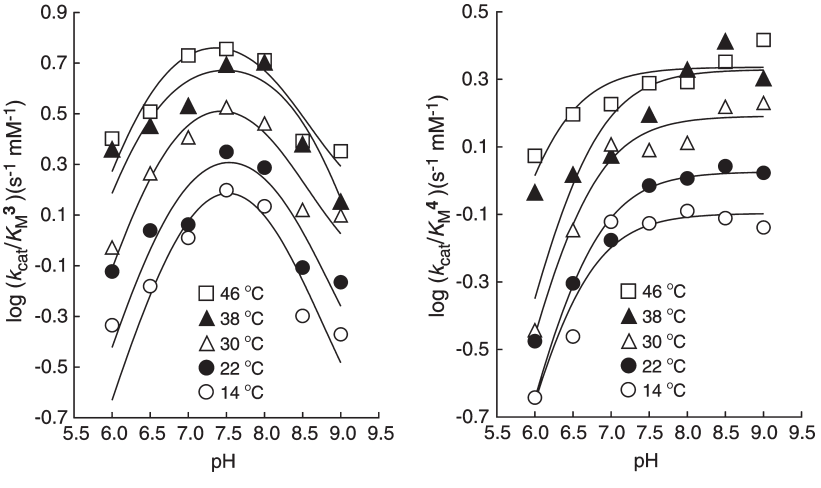

FIGURE 4: Effect of pH on k_{cat}/K_M for StEH1-catalyzed formation of **3** (A) or **4** (B) from epoxide **2**, at different temperatures. Fitted lines correspond to titrations involving two (A) or one (B) ionization event.

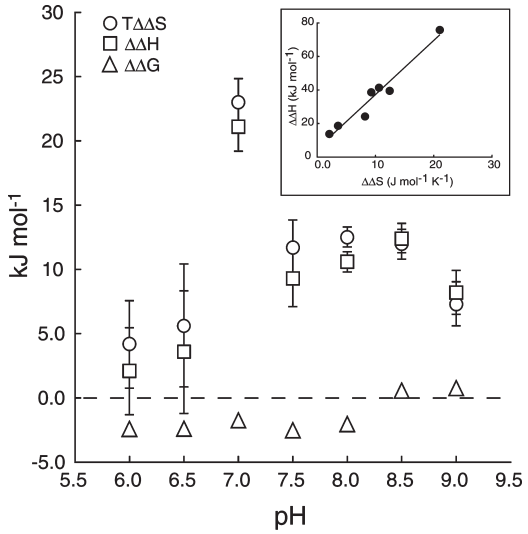

FIGURE 5: Differences in activation enthalpy, activation entropy, and Gibbs free energy in the reaction pathways leading to formation of the different diol enantiomers **3** or **4**. Inset: Linear correlation of the difference in activation enthalpy versus activation entropy, R^2 = 0.95.

enantiomers. These differences in binding modes are supported by the simulations with the HssEH where the altered positions of the substrate resulted in a different hydrogen-bonding pattern between substrate and enzyme (*51*).

The slight depression in the ratio of k_{cat}/K_M values seen at pH 7.0, as compared to neighboring pH values (Figure 3B), cannot presently be simply explained. The matrix of experimental values of k_{cat}/K_M for each product enantiomer (spanning pH 6.0−9.0 in one dimension and 14−46 °C in the other) has been repeated with 350 μM **2**, yielding the same experimental pattern (data not shown).

Thermodynamics in Regioselectivity. Differences in activation enthalpy, $\Delta_{3-4}\Delta H^{\ddagger}$, and activation entropy, $\Delta_{3-4}\Delta S^{\ddagger}$, derived from the ratios of the kinetic constant $(k_{cat}/K_M)^3/(k_{cat}/K_M)^4$, provide information on differences in catalytic steps and/or binding events. As stated before, StEH1 preferentially promotes attack at C-1 at pH values below 8.5, with activation entropy being the main contributor to the difference in activation energy (Figure 5). The enthalpy penalty is compensated by a positive entropy change (inset in Figure 5) which correlates linearly with an R^2 value of 0.95. The temperature dependences of activation enthalpy and entropy are similar but work in opposite directions. This causes a shift in preference toward attack at C-2 at pH ≥8.5, as the difference in activation enthalpy becomes the main contributor to the free energy differences. The temperature where the enzyme shows no selectivity, defined as the "reversal" temperature T_r, is obtained by dividing the activation enthalpy, $\Delta_{3-4}\Delta H^{\ddagger}$, with the activation entropy, $\Delta_{3-4}\Delta S^{\ddagger}$ (*53*). T_r increases with increasing pH (Supporting Information Table SI-5) in the StEH1-catalyzed hydrolysis of **2**. There are no simple relationships between low T_r values (at low pH) and high regioselectivity, confirming that regioselectivity is a complex function influenced by many factors.

In the noncatalyzed hydrolysis reactions the differences in activation enthalpy and entropy contributions in the transition states of the different reaction pathways differ from the enzyme-catalyzed reactions. A modified Eyring plot of ln([**3**]/[**4**]) versus $1/T$ results in a very small favorable negative difference in activation enthalpy over the whole pH range, accompanied by an increase in difference in activation entropy contribution with increasing pH (data not shown). This results in free energies of activation, $\Delta\Delta G^{\ddagger}$, ranging from −0.8 kJ mol^{-1} at pH 6.0 to −6 kJ mol^{-1} at pH 9.0. Hence, for the noncatalyzed reaction, the increased ratio of formation of **3** is primarily dependent on entropic factors favoring formation of the corresponding transition states.

The large errors associated with the thermodynamic parameters at pH <7.0 are caused by a nonlinear behavior in the Eyring plot (Supporting Information Figure SI-2) of ln $((k_{cat}/K_M)^3/(k_{cat}/K_M)^4)$ versus $1/T$. Below 30 °C the slope of the line corresponds to an activation enthalpy of −10 ± 3 kJ mol^{-1}, accompanied by a large negative activation entropy value of −25 ± 10 J K^{-1}·mol^{-1}. Above 30 °C the slope of the line of the least-squares fit is inversed, with the activation enthalpy changing sign to reach a value of 13 ± 2 kJ mol^{-1} while the entropy contribution is positive with a value of 50 ± 6 J K^{-1}·mol^{-1}. The resulting free energies of activation at 30 °C are negative with values corresponding to −2.4 and −1.8 kJ mol^{-1}, respectively. It has been suggested by Cainelli et al. that nonlinear Eyring plots of ln E vs $1/T$ can result from two different substrate−solvent clusters (*54*). As a structural shift between clusters takes place, the plots are inversed. In the present case T_{inv} takes place at 30 °C. Since the Eyring plots for the noncatalyzed reactions do not show this behavior, it may suggest that temperature-dependent conformational changes in the enzyme are the underlying cause for the nonlinearity.

Hysteresis, Cooperativity, and Promiscuous Regioselectivity. The rate-limiting step in StEH1-catalyzed hydrolysis of epoxides is in almost all examined cases alkyl enzyme hydrolysis (*3*, *12*). However, with epoxide **2** as substrate this has not been firmly established as the slow structural interconversions between E and E′ and/or ES and E′S (Scheme 1) are rate-limiting for alkyl enzyme formation (*12*). There are still no available experimentally determined structures with substrates bound in the active site, and none of the available crystal structures supports the presence of conformational changes affecting catalysis in epoxide hydrolases. However, Mowbray et al. reported on an adaptation of two segments at the "outside" of the active site cavity between different StEH1 proteins in the same unit cell resulting from binding of different ligands to the active sites (*50*). The segments involved in StEH1 overlap with the structural parts proposed by Shøitt to be in motion during catalysis of **1** in the murine epoxide hydrolase (*41*). Based on our presented results and the work by Shøitt and Mowbray et al., it is tempting to ponder on a linkage between regioselective promiscuity and slow conformational changes seen by the hysteretic kinetic behavior. The presence of conformational changes is supported by the fact that the differences in activation enthalpies are positive at all pH, as would be expected if the highest energy barrier would constitute a conformational step slower than all other steps in the catalytic cycle, i.e., hysteresis (*47*). We propose that these conformational changes are coupled to alternative binding modes of the epoxide substrate within the active site.

In our present working model of the kinetic mechanism we propose that free StEH1 exists in two different conformers in solution, interconverting with an equilibrium distribution depending on the values of k_0 and k_{-0}. The existence of both conformers will be observed in the pre-steady-state kinetics *if* the substrate can bind productively to both conformers *and* the subsequent reaction steps proceed through both pathways and are being diverged from ES to E′S (or the other way around) with

rate(s) (k_{-5} and/or k_5) lower or close to k_{cat} values. Regioselective promiscuity is a direct result of a conversion of a substrate into two product diols, as seen with epoxide **2**, but it does not necessarily need to be linked to hysteresis. However, from the negative substrate dependence observed in the pre-steady-state measurements with **2** it can be concluded that, in this case, hysteresis and regioselective promiscuity appear linked. Furthermore, if the sum of k_{-5} and k_5 is lower or equal to k_{cat}, it is likely that substrates traversing through E′S ⇌ ES will show hysteretic cooperativity in steady-state measurements.

CONCLUSIONS

We have shown that in promiscuous regioselectivity the preference of which carbon to attack can be manipulated more than 5-fold by altering the temperature and pH. A straightforward test of the temperature dependence on the product outcome, at two different pH values, provides a simple method to optimize reaction conditions in order to reach maximal product purity.

From the different pH dependencies seen in formation of diols **3** and **4** we propose that the causes for a high degree of regioselectivity are dependent on the positioning of the substrate within the active site cavity and that isomerization between these different conformers involves a conformational change in the enzyme. This proposal is supported by results from earlier simulation work (*13*, *40*) and the thermodynamic data presented here, with a positive activation enthalpy coupled to the formation of both enantiomers. Also, lower temperatures lead to relative increases in formation of diol **4** as compared to higher temperatures. During the later years there has been a growing awareness about the importance of dynamics in enzymatic catalysis, supported by both experiments and theoretical studies (*55*−*60*). The presence of conformational changes during the formation of the diols would suggest that dynamic properties of the enzyme can play an important role in enzyme-catalyzed hydrolysis of certain epoxides and contribute to the degree of regioselectivity.

In an earlier study on the hydrolysis of epoxide **2** we proposed a kinetic mechanism (Scheme 1) explaining epoxide hydrolase catalyzed hydrolysis of all substrates. The deviance from earlier models is mainly based on the hydrolysis of epoxide **2** forming both diol products **3** and **4** in a reaction where a hysteretic behavior was observed in the pre-steady-state kinetics. With this work we show that the same model includes the explanation of the promiscuous regioselectivity and hysteretic cooperativity.

ACKNOWLEDGMENT

The authors thank Mikael Holm for contributions to the project.

SUPPORTING INFORMATION AVAILABLE

The description of the parameters in the derived steady-state law, the complete equation used for fitting the pre-steady-state data, the Eyring plots of the difference in activation energy in the formation of **3** and **4**, tables with the k_{cat}/K_M or [**3**]/[**4**] for formation of enantiomers, and a table with the resulting thermodynamic data. This material is available free of charge via the Internet at http://pubs.acs.org.

REFERENCES

1. Yudin, A. K. (2006) Aziridines and epoxides in organic synthesis, Wiley-VCH Verlag, Weinheim, Germany.
2. Ollis, D. L., Cheah, E., Cygler, M., Dijkstra, B., Frolow, F., Franken, S. M., Harel, M., Remington, S. J., Silman, I., Schrag, J., Sussman, J. L., Verschueren, K. H. G., and Goldman, A. (1992) The alpha/beta hydrolase fold. *Protein Eng. 5*, 197–211.
3. Elfström, L. T., and Widersten, M. (2005) Catalysis of potato epoxide hydrolase, StEH1. *Biochem. J. 390*, 633–640.
4. Tzeng, H. F., Laughlin, L. T., and Armstrong, R. N. (1998) Semifunctional site-specific mutants affecting the hydrolytic half-reaction of microsomal epoxide hydrolase. *Biochemistry 37*, 2905–2911.
5. Rink, R., Kingma, J., Lutje Spelberg, J. H., and Janssen, D. B. (2000) Tyrosine residues serve as proton donor in the catalytic mechanism of epoxide hydrolase from *Agrobacterium radiobacter*. *Biochemistry 39*, 5600–5613.
6. Armstrong, R. N., and Cassidy, C. S. (2000) New structural and chemical insight into the catalytic mechanism of epoxide hydrolases. *Drug Metab. Rev. 32*, 327–338.
7. Moussou, P., Archelas, A., Baratti, J., and Furstoss, R. (1998) Microbiological transformations. Part 39: Determination of the regioselectivity occurring during oxirane ring opening by epoxide hydrolases: a theoretical analysis and a new method for its determination. *Tetrahedron: Asymmetry 9*, 1539–1547.
8. Faber, K., and Kroutil, W. (2002) Stereoselectivity in biocatalytic enantioconvergent reactions and a computer program for its determination. *Tetrahedron: Asymmetry 13*, 377–382.
9. Moussou, P., Archelas, A., Furstoss, R., and Baratti, J. C. (2000) Clues for the existence of two different epoxide hydrolase activities in the fungus *Beauveria bassiana*. *Enzyme Microb. Technol. 26*, 414–420.
10. Zeldin, D. C., Wei, S., Falck, J. R., Hammock, B. D., Snapper, J. R., and Capdevila, J. H. (1995) Metabolism of epoxyeicosatrienoic acids by cytosolic epoxide hydrolase: substrate structural determinants of asymmetric catalysis. *Arch. Biochem. Biophys. 316*, 443–451.
11. Bellucci, G., Chiappe, C., Cordoni, A., and Marioni, F. (1993) Substrate enantioselectivity in the rabbit liver microsomal epoxide hydrolase catalyzed hydrolysis of *trans* and *cis* 1-phenylpropene oxides. A comparison with styrene oxide. *Tetrahedron: Asymmetry 4*, 1153–1160.
12. Lindberg, D., Gogoll, A., and Widersten, M. (2008) Substrate-dependent hysteretic behavior in StEH1-catalyzed hydrolysis of styrene oxide derivatives. *FEBS J. 275*, 6309–6320.
13. Williamson, K. C., Morisseau, C., Maxwell, J. E., and Hammock, B. D. (2000) Regio- and enantioselective hydrolysis of phenyloxiranes catalyzed by soluble epoxide hydrolase. *Tetrahedron: Asymmetry 11*, 4451–4462.
14. Blée, E., and Schuber, F. J. (1992) Regio- and enantioselectivity of soybean fatty acid epoxide hydrolase. *J. Biol. Chem. 267*, 11881–11887.
15. Bellucci, G., Chiappe, C., Cordoni, A., and Marioni, F. (1994) Different enantioselectivity and regioselectivity of the cytosolic and microsomal epoxide hydrolase catalyzed hydrolysis of simple phenyl substituted epoxides. *Tetrahedron Lett. 35*, 4219–4222.
16. Hanzlik, R. P., Edelman, M., Michaely, W. J., and Scott, G. (1976) Enzymic hydration of [^{18}O]epoxides. Role of nucleophilic mechanisms. *J. Am. Chem. Soc. 98*, 1952–1955.
17. Hanzlik, R. P., Heideman, S., and Smith, D. (1978) Regioselectivity in enzymatic hydration of *cis*-1,2-disubstituted [^{18}O]-epoxides. *Biochem. Biophys. Res. Commun. 82*, 310–315.
18. Jerina, D. M., Ziffer, H., and Daly, J. W. (1970) Role of the arene oxide-oxepin system in the metabolism of aromatic substrates. IV. Stereochemical considerations of dihydrodiol formation and dehydrogenation. *J. Am. Chem. Soc. 92*, 1056–1061.
19. Kroutil, W., Mischitz, M., Plachota, P., and Faber, K. (1996) Deracemization of (±)-*cis*-2,3-epoxyheptane via enantioconvergent biocatalytic hydrolysis using *Nocardia* EH1-epoxide hydrolase. *Tetrahedron Lett. 37*, 8379–8382.
20. Kroutil, W., Mischitz, M., and Faber, K. (1997) Deracemization of (±)-2,3-disubstituted oxiranes via biocatalytic hydrolysis using bacterial epoxide hydrolases: kinetics of an enantioconvergent process. *J. Chem. Soc., Perkin Trans. 1*, 3629–3636.
21. Laughlin, L. T., Tzeng, H.-F., Lin, S., and Armstrong, R. N. (1998) Mechanism of microsomal epoxide hydrolase. Semifunctional site-specific mutants affecting the alkylation half-reaction. *Biochemistry 37*, 2897–2904.
22. Linderman, R. J., Walker, E. A., Haney, C., and Roe., R. M. (1995) Determination of the regiochemistry of insect epoxide hydrolase catalyzed epoxide hydration of juvenile hormone by ^{18}O-labeling studies. *Tetrahedron 51*, 10845–10856.
23. Mischitz, M., Mirtl, C., Saf, R., and Faber, F. (1996) Regioselectivity of *Rhodococcus* NCIMB 11216 epoxide hydrolase: applicability of *E*-values for description of enantioselectivity depends on substrate structure. *Tetrahedron: Asymmetry 7*, 2041–2046.

24. Nakamura, T., Nagasawa, T., Yu, F., Watanabe, I., and Yamada, H. (1994) Purification and characterization of two epoxide hydrolases from *Corynebacterium* sp. strain N-1074. *Appl. Environ. Microbiol. 60*, 4630–4633.
25. Pedragosa-Moreau, S., Archelas., A., and Furstoss, R. (1994) Microbiological transformations. XXIX. Enantioselective hydrolysis of epoxides using microorganisms: a mechanistic study. *Bioorg. Med. Chem. 2*, 609–616.
26. Niehaus, W. G., and Schroepfer, G. J. (1967) Enzymic stereospecificity in the hydration of epoxy fatty acids. Stereospecific incorporation of the oxygen of water. *J. Am. Chem. Soc. 89*, 4227–4228.
27. Dietze, E. C., Kuwano, E., Casas, J., and Hammock, B. D. (1991) Inhibition of cytosolic epoxide hydrolase by *trans*-3-phenylglycidols. *Biochem. Pharmacol. 42*, 1163–1175.
28. Zhang, X. M., Archelas, A., and Furstoss, R. (1991) Microbial transformations. 19. Asymmetric dihydroxylation of the remote double bond of geraniol: a unique stereochemical control allowing easy access to both enantiomers of geraniol-6,7-diol. *J. Org. Chem. 56*, 3814–3817.
29. Moussou, P., Archelas, A., and Furstoss, R. (1998) Microbiological transformations 41: screening for novel fungal epoxide hydrolases. *J. Mol. Catal. B: Enzym. 5*, 447–458.
30. Parker, R. E, and Isaacs, N. S. (1959) Mechanisms of epoxide reactions. *Chem. Rev. 59*, 737–799.
31. Whalen, D. L. (2005) Mechanisms of hydrolysis and rearrangements of epoxides. *Adv. Phys. Org. Chem. 40*, 247–298.
32. Arand, M., Cronin, A., Oesch, F., Mowbray, S. L., and Jones, T. A. (2003) The telltale structures of epoxide hydrolases. *Drug Metab. Rev. 35*, 365–383.
33. Morisseau, C., Beetham, J. K., Pinot, F., Debernard, S., Newman, J. W, and Hammock, B. D. (2000) Cress and potato soluble epoxide hydrolases: purification, biochemical characterization, and comparison to mammalian enzymes. *Arch. Biochem. Biophys. 378*, 321–332.
34. Cao, L., Lee, J., Chen, W., and Wood, T. K. (2006) Enantioconvergent production of (*R*)-1-phenyl-1,2-ethanediol from styrene oxide by combining the *Solanum tuberosum* and an evolved *Agrobacterium radiobacter* AD1 epoxide hydrolases. *Biotechnol. Bioeng. 94*, 522–529.
35. Simeó, Y., and Faber, K. (2006) Selectivity enhancement of enantio- and stereo-complementary epoxide hydrolases and chemo-enzymatic deracemization of (±)-2-methylglycidyl benzyl ether. *Tetrahedron: Asymmetry 17*, 402–409.
36. Manoj, K. M., Archelas, A., Baratti, J., and Furstoss, R. (2001) Microbiological transformations. Part 45: A green chemistry preparative scale synthesis of enantiopure building blocks of eliprodil: elaboration of a high substrate concentration epoxide hydrolase-catalyzed hydrolytic kinetic resolution process. *Tetrahedron 57*, 695–701.
37. Monterde, M. I., Lombard, M., Archelas, A., Cronin, A., Arand, M., and Furstoss, R. (2004) Enzymatic transformations. Part 58: Enantioconvergent biohydrolysis of styrene oxide derivatives catalysed by the *Solanum tuberosum* epoxide hydrolase. *Tetrahedron: Asymmetry 15*, 2801–2805.
38. Chiappe, C., Leandri, E., Lucchesi, S., Pieraccini, D., Hammock, B. D., and Morisseau, C. (2004) Biocatalysis in ionic liquids: the stereoconvergent hydrolysis of *trans*-β-methylstyrene oxide catalyzed by soluble epoxide hydrolase. *J. Mol. Catal. B: Enzym. 27*, 243–248.
39. Lotter, J., Botes, A. L., van Dyk, M. S., and Breytenbach, J. C. (2004) Hydrolytic kinetic resolution of the enantiomers of the structural isomers *trans*-1-phenylpropene oxide and (2,3-epoxypropyl)benzene by yeast epoxide hydrolase. *Biotechnol. Lett. 26*, 1197–1200.
40. Schiøtt, B., and Bruice, T. C. (2002) Reaction mechanism of soluble epoxide hydrolase: insights from molecular dynamics simulations. *J. Am. Chem. Soc. 124*, 14558–14570.
41. Schiøtt, B. (2004) Possible involvement of collective domain movement in the catalytic reaction of soluble epoxide hydrolase. *Int. J. Quantum Chem. 99*, 61–69.
42. Chen, C.-S., Fujimoto, Y., Girdaukas, G., and Sih, C. J. (1982) Quantitative analyses of biochemical kinetic resolutions of enantiomers. *J. Am. Chem. Soc. 104*, 7294–7299.
43. Straathof, A. J. J., and Jongejan, J. A. (1997) The enantiomeric ratio: origin, determination and prediction. *Enzyme Microb. Technol. 21*, 559–571.
44. Segel, I. H. (1975) Enzyme kinetics, pp 658−659, John Wiley & Sons, New York.
45. Masson, P., Schopfer, L. M., Froment, M.-T., Debouzy, J.-C., Nachon, F., Gillon, E., Lockridge, O., Hrabovska, A., and Goldstein, B. N. (2005) Hysteresis of butyrylcholinesterase in the approach to steady-state kinetics. *Chem.-Biol. Interact. 157*−*158*, 143–152.
46. Kim, Y. B., Kalinowski, S. S., and Marcinkeviciene, J. (2007) A pre-steady state analysis of ligand binding to human glucokinase: evidence for a preexisting equilibrium. *Biochemistry 46*, 1423–1431.
47. Neet, K. E., and Ainslie, G. R., Jr. (1980) Hysteretic enzymes. *Methods Enzymol. 64*, 192–226.
48. Frieden, C. (1979) Slow transitions and hysteretic behavior in enzymes. *Annu. Rev. Biochem. 48*, 471–489.
49. Lau, E. Y., Newby, Z. E., and Bruice, T. C. (2001) A theoretical examination of the acid-catalyzed and noncatalyzed ring-opening reaction of an oxirane by nucleophilic addition of acetate. Implications to epoxide hydrolases. *J. Am. Chem. Soc. 123*, 3350–3357.
50. Mowbray, S. L., Elfström, L. T., Ahlgren, K. M., Andersson, C. E., and Widersten, M. (2006) X-ray structure of potato epoxide hydrolase sheds light on substrate specificity in plant enzymes. *Protein Sci. 15*, 1628–1637.
51. Hopmann, K. H., and Himo, F. (2006) Theoretical study of the full reaction mechanism of human soluble epoxide hydrolase. *Chem.—Eur. J. 12*, 6898–6909.
52. Thomaeus, A., Carlsson, J., Åqvist, J., and Widersten, M. (2007) Active site of epoxide hydrolases revisited: a noncanonical residue in potato StEH1 promotes both formation and breakdown of the alkylenzyme intermediate. *Biochemistry 46*, 2466–2479.
53. Phillips, R. S. (1992) Temperature effects on stereochemistry of enzymatic reactions. *Enzyme Microb. Technol. 14*, 417–419.
54. Cainelli, G., Galletti, P., Giacomini, D., Gualandi, A., and Quintavalla, A. (2003) Chemo- and enzyme-catalyzed reactions revealing a common temperature-dependent dynamic solvent effect on enantioselectivity. *Helv. Chim. Acta 86*, 3548–3559.
55. Hammes, G. G. (2002) Multiple conformational changes in enzyme catalysis. *Biochemistry 41*, 8221–8228.
56. Agarwal, P. K. (2005) Role of protein dynamics in reaction rate enhancement by enzymes. *J. Am. Chem. Soc. 127*, 15248–15256.
57. Eisenmesser, E. Z., Millet, O., Labeikovsky, W., Korzhnev, D. M., Wolf-Watz, M., Bosco, D. A., Skalicky, J. J., Kay, L. E., and Kern, D. (2005) Intrinsic dynamics of an enzyme underlies catalysis. *Nature 438*, 117–121.
58. Hammes-Schiffer, S., and Benkovic, S. J. (2006) Relating protein motion to catalysis. *Annu. Rev. Biochem. 75*, 519–541.
59. Gerlt, J. A., and Babbitt, P. C. (2009) Enzyme (re)design: lessons from natural evolution and computation. *Curr. Opin. Chem. Biol. 13*, 10–18.
60. Tokuriki, N., and Tawfik, D. S. (2009) Protein dynamism and evolvability. *Science 324*, 203–207.